

Scaling Properties of Fluctuations in Human Electroencephalogram

Rudolph C. Hwa

*Institute of Theoretical Science and Department of Physics
University of Oregon, Eugene, OR 97403-5203, USA*

Thomas C. Ferree*

*Electrical Geodesics, Inc., Riverfront Research Park, Eugene, OR 97403
(May 30, 2018)*

The fluctuation properties of the human electroencephalogram (EEG) time series are studied using detrended fluctuation analysis. For all 128 channels in each of 18 subjects studied, it is found that the standard deviation of the fluctuations exhibits scaling behaviors in two regions. Topographical plots of the scaling exponents reveal the spatial structure of the nonlinear electrical activities recorded on the scalp. Moment analyses are performed to extract the gross features of all the scaling exponents. The correlation between the two scaling exponents in each channel is also examined. It is found that two indices can characterize the overall properties of the fluctuation behaviors of the brain dynamics for every subject and that they vary widely across the subjects.

PACS numbers: 05.45.Tp, 87.19.La, 87.90.+y

I. INTRODUCTION

The scalp electroencephalogram (EEG) provides a wealth of information about human brain dynamics. The complex nature of brain dynamics results in a high degree of fluctuations in both the spatial and temporal aspects of the EEG signals. To extract the salient properties from the data is the primary objective of any method of analysis. We present in this paper a novel method that explores the scaling behavior of the fluctuations and uses moment analysis to reduce the complexity of the results obtained.

The most common methods of EEG time series analyses are event-related time ensemble averaging and Fourier decomposition, both of which are based implicitly on assumptions of linearity [1,2]. Since the physiological mechanisms underlying the scalp EEG are generally nonlinear, they can generate fluctuations that are not best described by linear decomposition. Moreover, the resting EEG always displays a broad-banded power spectrum, so in Fourier analysis one must arbitrarily define frequency bands ($\delta, \theta, \alpha, \dots$) which may not actually delineate different dynamical mechanisms. Wavelet analyses have also been applied to examine EEG time series [3], but at a sacrifice of the ability to describe long-range temporal correlations. Chaos analyses have been applied to quantify the nonlinear behavior of the

brain [4–6], but typically require a long period of time to compute attractor properties for a single time series. Moreover, chaos-based approaches assume the existence of low-dimensional attractors, and this is probably not generally a valid assumption for the brain. In this paper, we discuss a method that analyzes the fluctuations in EEG over a short period of time (around 10s), and makes use of the information conveyed by all 128 channels on the scalp. We show the existence of scaling behaviors of certain measures of fluctuations in all channels and in all subjects. We propose two global measures of the spatio-temporal signals that characterize the distinctive nature of EEG for each subject.

The study of scaling behavior emphasizes the relationship across time scales. We aim to find what is universal among all channels as well as what varies among them. The former is obviously important by virtue of its universality for a given subject; how that universal quantity varies from subject to subject is clearly interesting. What varies from channel to channel is perhaps even more interesting, since it has implications for describing focal features which could have functional or clinical relevance.

Our procedure is to focus initially on one channel at a time. Thus it is a study of the local temporal behavior and the determination of a few parameters (scaling exponents) that effectively summarize the fluctuation properties of the time series. The second phase of our procedure is to describe the global behavior of all channels and to arrive at two numbers that summarize the variability of these temporal measures across the entire scalp surface. This dramatic data reduction necessarily trades detail for succinctness, but such reduction is exactly what is needed to allow easy discrimination between brain states.

The emphasis in this paper is on the method of analysis. It is not our aim here to perform clinical and cognitive analyses. Due to the fact that the EEG data available to us are short in time duration and few in the number of subjects studied, it is not feasible for us to make reliable inference on the physiological implications of our findings. Nevertheless, the data are sufficient for the extraction of interesting behaviors that are channel dependent as well as subject dependent.

II. DETRENDED FLUCTUATION ANALYSIS

The specific method we use in the first phase is detrended fluctuation analysis (DFA). This analysis is not new. It was proposed for the investigation of correlation properties in non-stationary time series and applied to the studies of heartbeat [7] and DNA nucleotides [8]. It has also been applied to EEG [9], but with somewhat different emphases than those presented here. Since the analysis considers only the fluctuations from the local linear trends, it is insensitive to spurious correlations introduced by non-stationary external trends. By examining the scaling behavior one can learn about the nature of short-range and long-range correlations.

Let an EEG time series be denoted by $y(t)$, where t is discrete time ranging from 1 to T . Divide the entire range of t to be investigated into B equal bins, discarding any remainder, so that each bin has $k = \text{floor}(T/B)$ time points. Within each bin, labeled b ($b = 1, \dots, B$), perform a least-square fit of $y(t)$ by a straight line, $\bar{y}_b(t)$, i.e., $\bar{y}_b(t) = \text{Linear-fit}[y(t)]$ for $(b-1)k < t \leq bk$. That is the semi-local trend for the b th bin. Define $F_b^2(k)$ to be the variance of the fluctuation $y(t)$ from $\bar{y}_b(t)$ in the b th bin, i.e.,

$$F_b^2(k) = \frac{1}{k} \sum_{t=(b-1)k+1}^{bk} [y(t) - \bar{y}_b(t)]^2 \quad (1)$$

It is a measure of the semi-locally detrended fluctuation in bin b . The average of $F_b^2(k)$ over all bins is

$$F^2(k) = \frac{1}{B} \sum_{b=1}^B F_b^2(k). \quad (2)$$

$F(k)$ is then the RMS fluctuation from the semi-local trends in B bins each having k time points.

The study of the dependence of $F(k)$ on the bin size k is the essence of DFA [7,8]. If it is a power-law behavior

$$F(k) \propto k^\alpha, \quad (3)$$

then the scaling exponent α is an indicator of the correlations of the fluctuations in EEG, which depends on the relationship of these fluctuations across time scales. Since DFA considers only the fluctuations from the semi-local linear trends, it is insensitive to spurious correlations introduced by non-stationary external trends. This is a practical advantage since EEG acquisition systems often suffer from slow drifts associated with gradual changes in the quality of electrode contact to the skin. The analysis also liberates our result from the dependence on the overall magnitude of the voltage $y(t)$ recorded by each probe, which is an advantage since overall signal amplitude can vary across subjects, presumably due to differences in skull conductivity and other factors.

Resting EEG data were collected for 18 subjects using a 128-channel commercial EEG system, with scalp-electrode impedances ranging from 10 to 40 k Ω . The

data were hardware filtered between 0.1 and 100 Hz, then digitized at 250 points/sec. After acquisition, $T \approx 10$ s lengths of simultaneous time series in all channels are chosen, free of artifacts such as eye blink and head movements. At each time point, the average across all electrodes was subtracted, to remove approximately the effect of the reference electrode [2]. We investigate the range of k from 3 to 500 in approximately equal steps of $\ln k$.

In Fig. 1 we show three typical time series $y(t)$ in three widely separated channels for subject A, labeled 1-3, for brevity. While it is clear that both channels 2 and 3 have substantial 10 Hz oscillations after 0.2s, it is much less apparent that there exist any scaling behaviors in all three channels. The corresponding values of $F(k)$ are shown in the log-log plot in Fig. 2. Evidently, the striking feature is that there are two scaling regions with a discernible bend when the two slopes in the two regions are distinctly different. With rare exceptions this feature is found in all channels for all subjects. Admittedly, the extents of the scaling regions are not wide, so the behavior does not meet the qualification for scaling in large critical systems or in fractal geometrical objects. However, since the behavior is so universal across channels and subjects, and since the temporal scales involved are physiologically relevant, the scaling behavior is a feature of EEG that conveys an important property of the brain activity and should not be overlooked.

III. SCALING AND NONSCALING PROPERTIES

The fact that there exist two scaling regions suggests that the lack of scaling in the region between the two implies the existence of some significant time scale. From Fig. 1 one indeed sees roughly periodic oscillations in Ch. 2 and 3. One may therefore be tempted to think that if, instead of considering the fluctuations from the linear semi-local trends $\bar{y}_b(t)$, one studies the fluctuations from periodic oscillations, then the bend would disappear and the two scaling regions might be joined to become one. However, even if that were true, such a procedure should not be used for two reasons. First, not all channels exhibit obvious oscillatory behaviors with definite frequencies. Channel 1 in Fig. 1 is one such example. Whatever detrending one chooses should be universally applied to all channels in order to avoid introducing discrepancies across the channels due to external intervention. Second, to determine the frequency of the oscillatory trend requires a Fourier analysis, which is precisely what our approach attempts to circumvent. To decide on a sinusoidal wave of a particular frequency as reference for detrending involves arbitrariness and is unlikely to lead to any simplification in the global picture. The simplest and unbiased approach is to use the semi-local linear trends, as we have done.

To quantify the scaling behavior, we perform a linear

fit in Region I for $1 < \ln k < 2.5$ and denote the slope by α_1 , and similarly in Region II for $3.5 < \ln k < 5.75$ with slope denoted by α_2 . Visual inspection for each of the 18 subjects verifies that fitting this way does a remarkably good job of characterizing the slopes in the two regions. Knowing the two straight lines in each channel allows us to determine the location of their intercept, $\ln \kappa$, which gives a good approximation for the position of the bend in $\ln k$. We find that, whereas α_1 and α_2 can fluctuate widely from channel to channel, κ is limited to a narrow range in most subjects. The average value of $\ln \kappa$ for each subject ranges from 2.6 to 3.6, with a grand average across subjects to be approximately 3.1. It should, however, be noted that when α_1 and α_2 are nearly the same, as is the case for Ch. 1 in Fig. 2, the determination of κ by the intersection of the two straight lines is not reliable. Nevertheless, it is visually clear that the bend occurs in the vicinity of $\ln \kappa = 3.1$.

Since scaling behavior means that the system examined has no intrinsic scale, scale noninvariance at κ implies that κ is related to a dominant frequency of oscillation in the time series. It is at this point that a contact can be made with the usual Fourier analysis. Although our analysis focuses on scale invariant quantities, i.e., the dimensionless scaling exponents, it is worth digressing momentarily to establish this contact. To do this, we loosely associate the time scale κ with the period of a sine wave with frequency f . If the data acquisition rate is denoted by r , then the frequency f corresponding to κ is

$$f = r/\kappa. \quad (4)$$

For our data acquisition we have $r = 250$ points/sec. For the across-subject average of $\ln \kappa = 3.1$, we get from Eq. (4) $f = 11.3$ Hz. That is in the middle of the traditional α (8-13 Hz) EEG frequency band. Thus the dominant periodic oscillation apparent in Fig. 1 does reveal itself in the study of the scaling behavior. If one's interest is in the frequency content of the EEG time series, then Fourier analysis is more direct. However, if the interest is in the fluctuation properties and their relationships across time scales, then DFA is more effective. Hereafter, frequency will play no essential role in the remainder of this paper.

For each subject we have 128 pairs of values of (α_1, α_2) , which summarize the temporal fluctuations in terms of scaling exponents. In Fig. 3, we exhibit by scatter plot the values of α_1 and α_2 of all channels for subject A. The three points marked with circles correspond to the channels shown in Fig. 2. The error bars in Fig. 3 indicate the goodness of fit of the two regions by straight lines. Since the variability of the scaling exponents across channels is large compared to the error in fit, the different values convey numerically meaningful information. For this subject, Region I exhibits better scaling behavior than Region II, although the error bars on α_2 are not so large as to call into question the power-law description in Region II.

Overall, for subject A, the scaling exponents are in the ranges: $0.19 < \alpha_1 < 1.44$ and $0.018 < \alpha_2 < 0.489$. Whereas α_1 is widely distributed, α_2 is sharply peaked at 0.1 and has a long tail. The value of $\alpha = 0.5$ corresponds to random walk with no correlation among the various time points. For $\alpha \neq 0.5$ there are correlations: Region I corresponds to short-range correlation, Region II long-range, with κ giving a quantitative demarkation between the two. In most channels we find $\alpha_1 > \alpha_2$, although there are a few where $\alpha_1 \approx \alpha_2$. The scatter plots of all other subjects are similar in general features to the one shown in Fig. 3, but vary in detail from subject to subject. It is impractical to show them all in this paper. Evidently, it is desirable to find a way to quantify succinctly these 128 pairs of numbers so that one can effectively compare the results across subjects.

A scatter plot such as Fig. 3 reveals very well how the α_i exponents of all the channels are related to one another. However, it shows nothing about the locations of the channels on the scalp. To show that, we use the topographical plots of α_1 and α_2 separately, as in Fig. 4, to exhibit the spatial structure of the signals extracted. The dissociation of α_1 from α_2 is a price paid to gain the spatial perspective on the scalp. Topographic plots such as this may be useful for specifying the location of focal features, e.g., associated with particular brain functions and/or pathologies. Thus topographical and scatter plots present different aspects of the fluctuation properties of the brain electrical activity of any given subject. Both are inefficient for comparison across subjects. What we need is a global measure that describes the general, overall feature of all α_i pairs in the form of a single parameter.

IV. MOMENTS OF THE SCALING EXPONENTS

We propose to consider the moments of the scaling exponents. In general, if we have N numbers, $z_j, j = 1, \dots, N$, we can calculate the moments

$$G_q = \frac{1}{N} \sum_{j=1}^N z_j^q, \quad (5)$$

where q is a positive integer [10]. The information contained in the first N moments (i.e., $q = 1, \dots, N$) is enough to reproduce all the z_j by inversion. However, we may be interested in only a few of the G_q with lower order q , each of which contains some information of all the z_j . In our present problem we have $N = 128$, and we shall consider the first ten orders, $1 \leq q \leq 10$. That is a significant reduction of numbers, a process worth investigating.

Before calculating the moments of α_i , let us see how those values are distributed. Let x be either α_1 or α_2 . Since no value of α_i has been found to exceed 1.5 in the subjects we have examined, we consider the interval $0 \leq x \leq 1.5$. Divide that interval into M equal cells,

which for definiteness we take to be $M = 150$ here. Let the cells be labeled by $m = 1, \dots, M$, each having the size $\delta x = 1.5/M$. Denote the number of channels whose x values are in the m th cell by n_m . Define

$$P_m = n_m / N. \quad (6)$$

It is the fraction of channels whose x values are in the range $(m-1)\delta x \leq x < m\delta x$. By definition, we have $\sum_{m=1}^M P_m = 1$. In Fig. 5 we show as an illustration the two graphs of P_m for subject A. The two graphs correspond to α_1 and α_2 , and are, in essence, the projections of the scatter plot in Fig. 3 onto the α_1 and α_2 axes. From Fig. 5 we see that α_1 is widely distributed, while α_2 is not. G_1 gives the average, and G_2 is related to the width.

Since the fluctuation of m in P_m should be measured relative to its mean, let us consider the normalized moments [11]

$$M_q^{(i)} = G_q^{(i)} / \left(G_1^{(i)}\right)^q = \sum_{m=1}^M m^q P_m^{(i)} / \left(\sum_{m=1}^M m P_m^{(i)}\right)^q, \quad (7)$$

where $i = 1$ or 2 . Since these moments are averages of $(m/\bar{m})^q$, where \bar{m} is the average- m , they are not very sensitive to \bar{m} itself. They contain the essence of the fluctuation properties of $\alpha_{1,2}$ in all channels. In terms of the scaling exponents explicitly, let us use $\alpha_i(j)$ to denote the value of α_i for channel j so that Eq.(7) may be rewritten as

$$M_q^{(i)} = \frac{1}{N} \sum_{j=1}^N \alpha_i(j)^q / \left(\frac{1}{N} \sum_{j=1}^N \alpha_i(j)\right)^q. \quad (8)$$

In principle, it is possible to examine also the moments for $q < 0$, which would reveal the properties of P_m at low values of m . However, the accuracy of our data is not too reliable for low- k analysis, since the 60 Hz noise due to ambient electric and magnetic fields has not been cleanly filtered out. In this paper, therefore, we restrict our study to only the positive q values. For high q , the large m/\bar{m} parts of $P_m^{(1,2)}$ dominate $M_q^{(1,2)}$.

In Fig. 6 the q -dependences of $\ln M_q^{(1,2)}$ are shown for the distributions exhibited in Fig. 5 for $2 \leq q \leq 10$. They are approximately linear except for the low values of q . The same type of dependencies on q are found for all subjects. In Fig. 6 we show two straight lines that can fit very well the nearly linear behaviors of $\ln M_q^{(i)}$ vs q for $q \geq 5$. Thus for large q we have

$$M_q^{(i)} \propto \exp(\mu_i q), \quad q \geq 5. \quad (9)$$

The linear extrapolations of the lines to lower values of q show the degree of deviation of the the calculated values of $\ln M_q^{(1,2)}$ from linearity. Since $\ln M_q^{(1)}$ and $\ln M_q^{(2)}$

behave so similarly in their departures from the linear dependencies on q , we plot $\ln M_q^{(2)}$ vs $\ln M_q^{(1)}$ in order to exhibit their direct relationship without explicit dependence on q . We find that they are linearly related over a wider range of values. This linearity is found to be true for all subjects. The plots for three of them are illustrated in Fig. 7, where the straight lines are the linear fits. Thus the implication is that there exists a universal power-law behavior

$$M_q^{(2)} \propto \left(M_q^{(1)}\right)^\eta \quad (10)$$

valid for all subjects examined. From Eqs.(9) and (10) we obtain

$$\eta = \mu_2 / \mu_1, \quad (11)$$

but now η is meaningful for all q (except for the lowest points) and in that sense independent of q . Thus we have discovered a global measure η that characterizes all α_i values of a subject, and varies from subject to subject. We postpone the display of all the η values for all subjects until later.

To understand the exponential behavior in Eq.(9), we note that G_q is dominated by large z_j when q is large, as is self-evident in Eq.(5). For asymptotically large q , we have $G_q \propto \exp(q \ln z_{\max})$, where $z_{\max} = \max\{z_j\}$. For intermediate q , all large values of z_j can make important contributions, and the exponential dependence on q can still prevail. The denominator in Eq.(7) is $G_1^q = \bar{z}^q = \exp(q \ln \bar{z})$, where \bar{z} is the average of z_j , so it is also exponential for any q . It is therefore clear that Eq.(9) follows, and that μ_i depends on all z_j with more weight on the large z_j values. The power-law behavior of Eq.(10) implies that the exponent η is independent of q and that all α_i values are relevant contributors to the universal behavior. This is an important point worth emphasizing: the independence of η on q implies that the whole spectra of α_1 and α_2 are summarized by the one index η . The fact that η varies from subject to subject is a consequence of the variability of all 128 pairs of (α_1, α_2) across the subjects, and offers the possibility that η can be used as a discriminating representation of the brain state.

V. CORRELATIONS OF THE SCALING EXPONENTS

The analysis in the preceding section treats the moments of α_1 and α_2 separately. Only in the last step are the global properties embodied in $M_q^{(1)}$ and $M_q^{(2)}$ related through the exponent η in Eq.(10). In that approach the pairing of α_1 with α_2 in each channel is not taken into account. However, we know that there are channels, such as Ch. 1 in Figs. 1 and 2, where the absence of a dominant mode of oscillation results in $\alpha_1 \approx \alpha_2$. Thus the

correlation between the two scaling exponents is an important feature that should be explored and quantified. To that end we define

$$\beta = \alpha_2/\alpha_1 \quad (12)$$

for each channel. In most cases we have $\beta < 1$, but $\beta > 1$ is possible and, by its rarity, noteworthy.

From a scatter plot, such as Fig. 3, it is possible to visualize the β distribution, since β is just the slope of a line from the origin to each point. We show in Fig. 8 the β distributions for the same three subjects as those in Fig. 7. Subject B is chosen for display because it has the largest η , while subject C is chosen because it has several β values that exceed 1.

To summarize the 128 values of β_j for each subject, we apply to them the moment analysis that is developed in Sec. IV. Let us therefore define

$$N_q = \frac{1}{N} \sum_{j=1}^N \beta_j^q \bigg/ \left(\frac{1}{N} \sum_{j=1}^N \beta_j \right)^q. \quad (13)$$

The q dependence of $\ln N_q$ for the same three subjects are shown in Fig. 9. Again, linear fits are very good. Thus we have

$$N_q \propto \exp(\nu q) \quad (14)$$

with a distinct ν for each subject. Clearly, the ones with wide β distributions relative to their means have higher values of ν .

We now have found two indices, η and ν , for each subject. They describe different aspects of the scaling exponents. To display those values, it is illuminating to show the scatter plot of (η, ν) , as in Fig. 10, which has 18 points for the 18 subjects studied. The subjects A, B and C are denoted by distinct symbols, same as in Fig. 9. We see that the points in Fig. 10 appear to form a band, roughly correlated in η and ν . Only subject C has a value of ν that lies above the band, and it is C who has several β values above 1. Whether that is an anomaly carrying some physiological significance is an issue outside the scope of this paper, since we assume no knowledge of the physical conditions of the subjects. We are similarly ignorant at this point about the meaning of the spread of the (η, ν) values. However, it is encouraging that the scatter plot in (η, ν) is widely distributed for the 18 subjects, since it offers the possibility of being a discriminating tool, quite different from the alternative scenario, if the parameters determined in an analysis had turned out to be nearly the same for all subjects.

VI. CONCLUSION

Recognizing that the brain is a highly nonlinear system, we have explored a possible way of analyzing the EEG time series that avoids the assumptions made in

linear analyses and in chaos studies. By studying the fluctuations from linear trends defined over varying time scale, we have found two scaling regions in which the RMS fluctuations can be characterized by two dimensionless scaling exponents, α_1 and α_2 , for each channel. We then performed moment analyses to reduce the large number of pairs of (α_1, α_2) to simple and manageable forms. The two types of independent moments, $M_q^{(i)}$ and N_q , yield two indices, η and ν , which provide concise signatures of the nonlinear behavior of all channels of the EEG signals.

Our emphasis in this paper has been on the method of analysis rather than on the physiological interpretation of the results. For the latter task it is necessary to have not only more data, but also detailed information on the physical conditions of the subjects so as to have a reference frame to calibrate the indices obtained. However, working with 18 subjects is sufficient to demonstrate the effectiveness of the method, to show the universality of the scaling behaviors, to reveal the range of variability of the indices derived, and to offer the possibility of a new way of understanding human brain activity.

Acknowledgment

We are grateful to Prof. Don Tucker and Dr. Phan Luu for supplying the EEG data for our analysis. We have also benefited from the computational assistance of Wei He. This work was supported, in part, by the U. S. Department of Energy under Grant No. DE-FG03-96ER40972, and the National Institutes of Health under Grant No. R44-NS-38829.

* Present address: Dynamic Neuroimaging Laboratory, Department of Radiology, University of California at San Francisco, San Francisco, CA 94143.

- [1] *Electroencephalography: Basic Principles, Clinical Applications, and Related Fields*, edited by E. Niedermeyer and F. H. Lopes da Silva (Urban and Schwarzenberg, Baltimore, 1987); *ibid* (Williams and Wilkins, Baltimore, 1998).
- [2] P. L. Nunez, *Neocortical Dynamics and Human EEG Rhythms* (Oxford University Press, 1995).
- [3] S. Blanco, C. D'Attellis, S. Isaacson, O. A. Rosso, and R. Sirne, *Phys. Rev. E* **54**, 6661 (1996); S. Blanco, A. Figliola, R. Quian Quiroga, O. A. Rosso, and E. Serrano, *Phys. Rev. E* **57**, 932 (1998).
- [4] *Chaos in Brain?*, edited by K. Lehnertz, J. Arnhold, P. Grassberger and C. E. Elger (World Scientific, Singapore, 2000).
- [5] B. H. Jansen and M. E. Brandt, *Nonlinear Dynamical Analysis of the EEG* (World Scientific, Singapore, 1993).
- [6] K. Lehnertz and C. E. Elger, *Phys. Rev. Lett.* **80**, 5019 (1998).
- [7] C.-K. Peng, S. Havlin, H. E. Stanley, and A. L. Goldberger, *Chaos* **5**, 82 (1995).
- [8] C.-K. Peng, S. V. Buldyrev, S. Havlin, M. Simons, H. E. Stanley, and A. L. Goldberger, *Phys. Rev. E* **49**, 1685 (1994).
- [9] Watters, P. A. *Complexity International* **5**, 1 (1998).
- [10] C. W. Gardiner, *Handbook of Stochastic Methods* (Springer-Verlag, Berlin, 1983).
- [11] R. C. Hwa, *Phys. Rev. D* **41**, 1456 (1990).

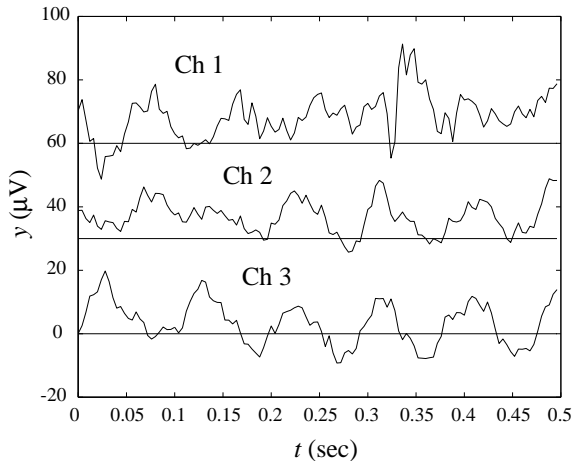


FIG. 1. A sample of EEG time series in three channels. The vertical scales of Ch. 1 and Ch. 2 are shifted upward by 60 and 30 μV , respectively.

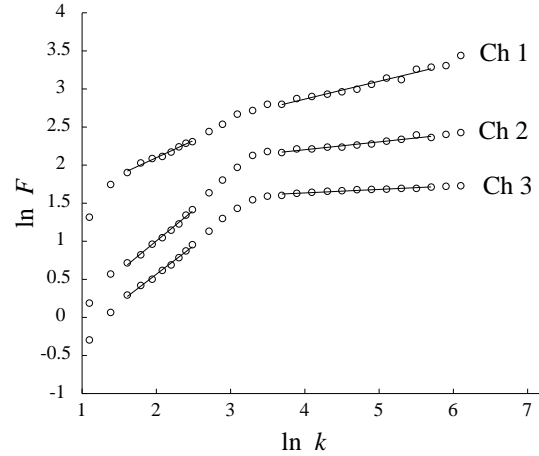


FIG. 2. $F(k)$ vs k for the three channels in Fig. 1. The vertical scales of Ch. 1 and Ch. 2 are shifted upwards by 1.0 and 0.5 units, respectively.

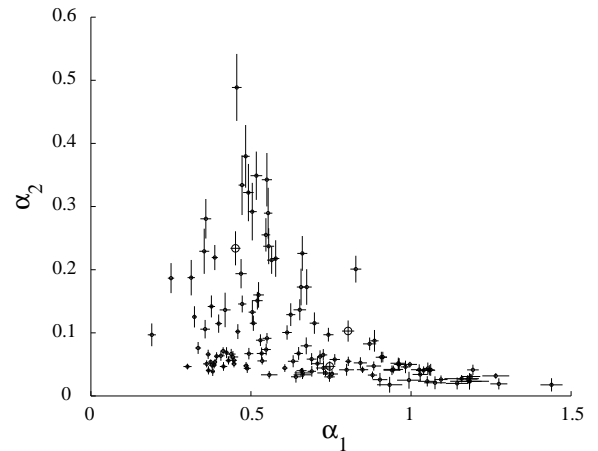


FIG. 3. Scatter plot of α_2 vs α_1 for subject A. The three channels exhibited in Figs. 1 and 2 are shown as circles.

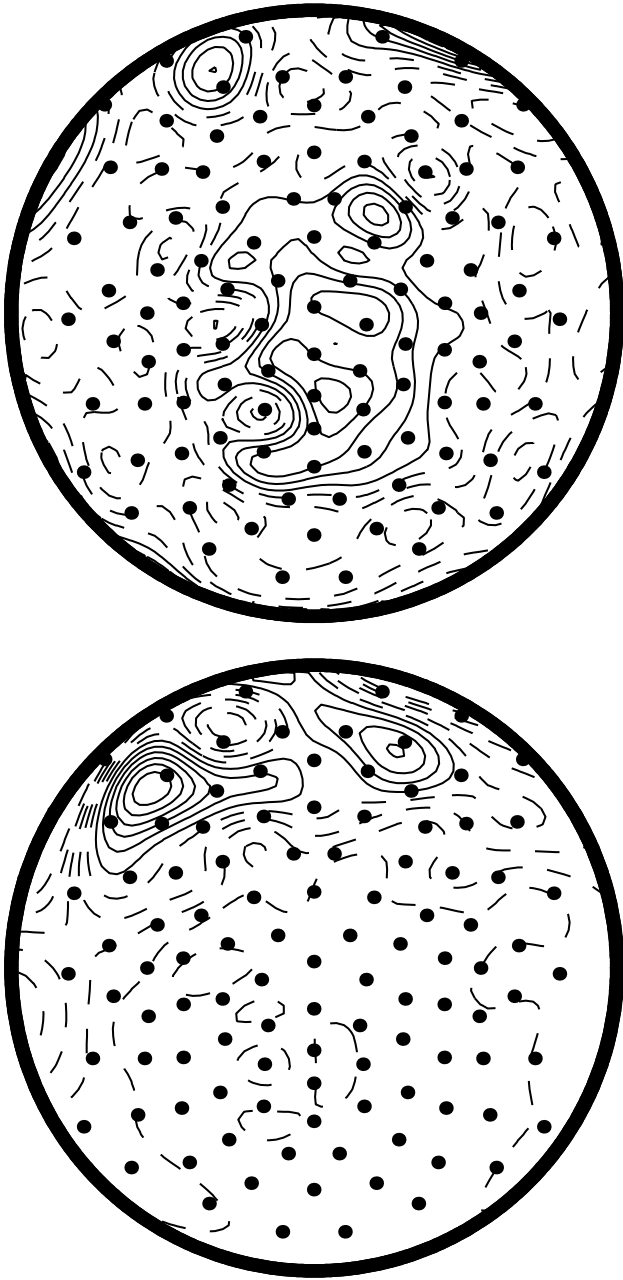


FIG. 4. Topographical plots of α_1 (top) and α_2 (bottom). In each figure, ten contour lines are drawn within the data range: solid lines above the mean, dotted lines below.

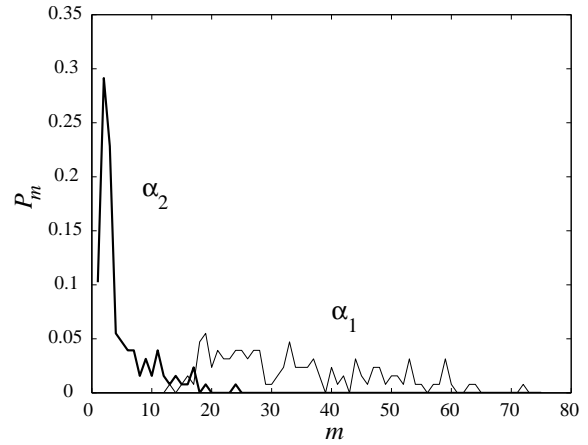


FIG. 5. The distributions P_m for α_1 and α_2 . The bin size in α for this plot is 0.02.

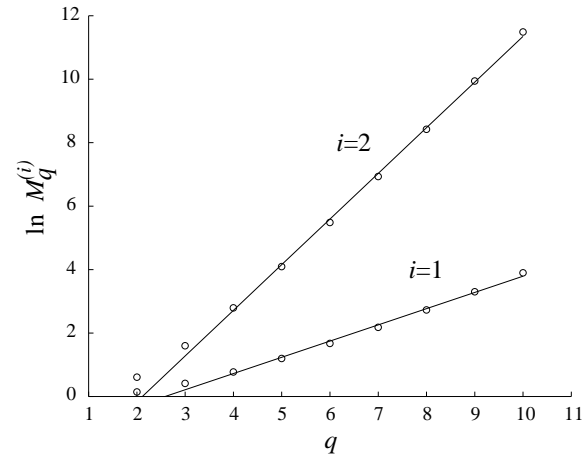


FIG. 6. The q dependence of $\ln M_q^{(i)}$ for subject A. The straight lines are linear fits of the points for $q \geq 5$.

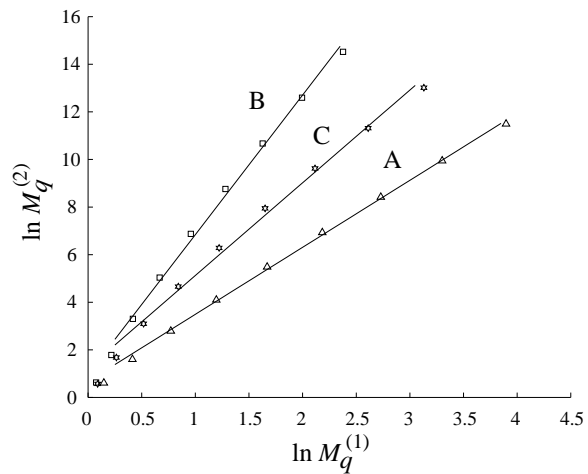


FIG. 7. A log-log plot of $M_q^{(2)}$ vs $M_q^{(1)}$ for three subjects A, B, and C. The solid lines have the slopes given by Eq. (11).

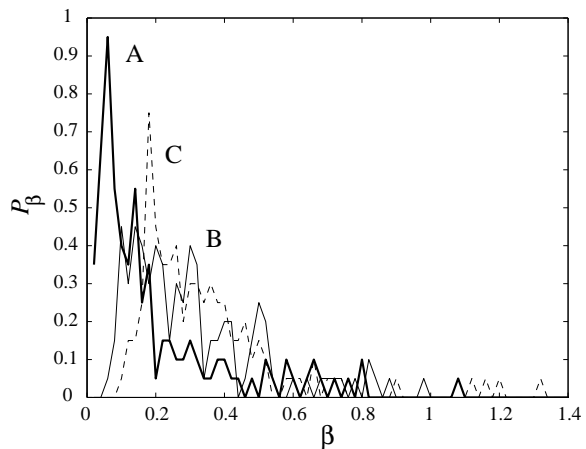


FIG. 8. The distributions of the β values of the subjects A, B, and C.

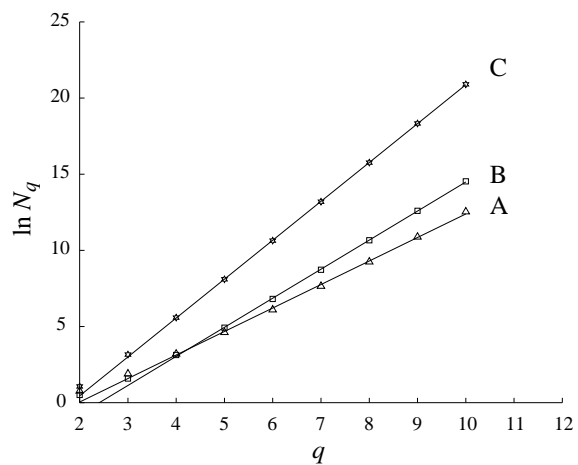


FIG. 9. The q dependence of $\ln N_q$ for subjects A, B, and C.

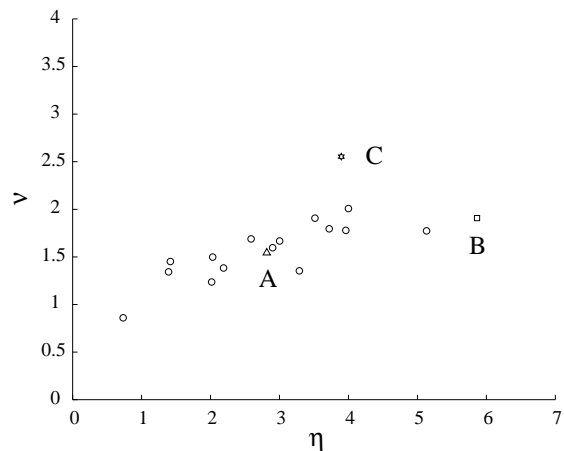


FIG. 10. Scatter plot of ν vs η for all 18 subjects, three of which have individual symbols: triangle (A), square (B), and star (C).